

Ultrafast Charge Migration in XUV Photoexcited Phenylalanine: a First-Principles Study Based on Real-Time Nonequilibrium Green's Functions

E. Perfetto,^{1,2} D. Sangalli,¹ A. Marini,¹ and G. Stefanucci^{2,3}

¹*CNR-ISM, Division of Ultrafast Processes in Materials (FLASHit),
Area della Ricerca di Roma 1, Via Salaria Km 29.3, I-00016 Monterotondo Scalo, Italy*

²*Dipartimento di Fisica, Università di Roma Tor Vergata,
Via della Ricerca Scientifica 1, 00133 Rome, Italy*

³*INFN, Sezione di Roma Tor Vergata, Via della Ricerca Scientifica 1, 00133 Rome, Italy**

The early stage density oscillations of the electronic charge in molecules irradiated by an attosecond XUV pulse takes place on femto- or subfemtosecond timescales. This ultrafast charge migration process is a central topic in attoscience as it dictates the relaxation pathways of the molecular structure. A predictive quantum theory of ultrafast charge migration should incorporate the atomistic details of the molecule, electronic correlations and the multitude of ionization channels activated by the broad-bandwidth XUV pulse. In this work we propose a first-principles Non Equilibrium Green's Function method fulfilling all three requirements, and apply it to a recent experiment on the photoexcited phenylalanine aminoacid. Our results show that dynamical correlations are necessary for a quantitative overall agreement with the experimental data. In particular, we are able to capture the transient oscillations at frequencies 0.15 PHz and 0.30 PHz in the hole density of the amine group, as well as their suppression and the concomitant development of a new oscillation at frequency 0.25 PHz after about 14 femtoseconds.

Photoinduced charge transfer through molecules is the initiator of a large variety of chemical and biological processes^{1–5}. Remarkable examples are the charge separation in photosynthetic centers, photovoltaic blends and catalytic triads or the radiation-induced damage of biological molecules. These phenomena occur on timescales of several tens of femtoseconds to picoseconds and, in general, the coupling of electrons to nuclear motion cannot be discarded^{6–8}. However, the density oscillations of the electronic charge following an attosecond XUV pulse precedes any structural rearrangement and takes place on femto- or subfemtosecond timescales. This early stage dynamics is mainly driven by electronic correlations⁹ and it is usually referred to as ultrafast *charge migration*. Charge migration dictates the relaxation pathways of the molecule, e.g., the possible fragmentation channels of the cations left after ionization¹⁰. Understanding and controlling this early stage dynamics has become a central topic in ultrafast science^{11,12} as it would, in principle, allow us to influence the ultimate fate of the molecular structure.

The sub-femtosecond electron dynamics in photoexcited or photoionized molecules can be probed in real-time with a number of experimental techniques, e.g., high-harmonic spectroscopy¹³, laser streaking photoemission¹⁴ or (fragment) cation chronoscopy^{10,15,16}. On the theoretical side, the description of ultrafast charge migration in attosecond XUV ionized molecules is a complex problem since the parent cation is left in a coherent superposition of several many-electron states⁵. In fact, the XUV-pulse bandwidth is as large as tens of eV, thus covering a wide range of ionization thresholds. The resulting oscillations of the charge density do therefore depend in a complicated manner on the electronic structure of the molecule and on the profile parameters of the laser pulse (intensity, frequency, duration).

Understanding ultrafast charge migration at a fundamental level inevitably requires a time-dependent (TD) quantum framework able to incorporate the atomistic details of the molecular structure. The numerical solution of the TD Schrödinger equation (SE) in the subspace of carefully selected many-electron states is certainly feasible for atoms but it becomes prohibitive already for diatomic molecules. Fortunately, many physical observables require only knowledge of the TD charge density $n(\mathbf{r}, t)$ [or the single-particle density matrix $\rho(\mathbf{r}, \mathbf{r}', t)$] rather than the full many-electron wavefunction. Density functional theory (DFT) and its TD extension^{17,18} are first-principles methods having $n(\mathbf{r}, t)$ as basic variable. TD-DFT calculations scale linearly with the number of electrons (against the exponential scaling of configuration interaction calculations) and it has been successfully applied to study ultrafast charge migration during and after photoionization in a number of molecules^{19–25}. Although TD-DFT is an exact reformulation of the TD-SE, in practice all simulations are carried out within the *adiabatic approximation*, i.e., by using the equilibrium DFT exchange-correlation (xc) potential evaluated at the instantaneous density $n(\mathbf{r}, t)$. The adiabatic approximation lacks of *dynamical exchange-correlation* effects which often play a major role in charge migration processes. For instance, ultrafast charge migration in different polypeptide molecules would not be possible without dynamical correlations.^{26–28} Double (or multiple) excitations^{29,30} and ionizations³¹, long-range charge transfer excitations^{32–34}, image-charge quasi-particle renormalizations^{35–37} and Auger decays³⁸ are other processes missed by the adiabatic approximation.

In this paper we take a step forward and propose a first-principles approach that shares with TD-DFT the favourable (power-law) scaling of the computational cost with the system size but, at the same time, allows for the

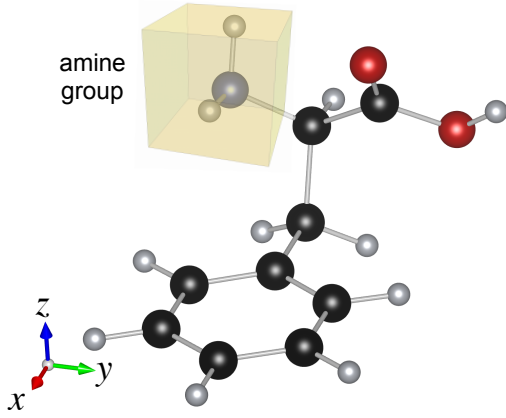


FIG. 1. Molecular structure of the most abundant conformer of the phenylalanine molecule, see Ref. 10. Black spheres represent carbon atoms; gray spheres, hydrogen atoms; blue sphere, nitrogen; and red spheres, oxygen. The amine group NH_2 is contained in a light-yellow cubic box.

inclusion of dynamical correlations in a *systematic* and *self-consistent* manner. The approach is based on Non Equilibrium Green's Functions (NEGF) theory^{31,39–45} and at its core is the (nonlinear) equation of motion for the single-particle density matrix ρ in the Kohn-Sham (KS) basis.

The NEGF method is applied to revisit and complement the TD-DFT analysis of ultrafast charge migration in the phenylalanine aminoacid reported in Ref. 10, see Fig. 1 for an illustration of the molecular structure. In the experiment the ultrafast electron motion is activated by an ionizing XUV 300-as pulse and it is subsequently probed by a VIS/NIR pulse. The probe causes a second ionization of the phenylalanine that eventually undergoes a fragmentation reaction. The yield $Y(\tau)$ of immonium dications is recorded for different pump-probe delays τ . The data show that for $\tau \lesssim 14$ fs the yield oscillates with a dominant frequency $\Omega_0^{\text{exp}} \approx 0.14$ PHz ($1 \text{ PHz} = 10^{15} \text{ Hz}$) and a sub-dominant one $\Omega_2^{\text{exp}} \approx 0.3$ PHz. For $\tau \gtrsim 14$ fs, instead, $Y(\tau)$ oscillates almost monochromatically at the frequency $\Omega_1^{\text{exp}} \approx 0.24$ PHz. Ref. 10 and other works⁴⁶ suggest that the yield of immonium dications shares common features with the TD hole density on the amine group NH_2 , see Fig. 1, driven by the action of the XUV only. This relation is also suggested by other experimental studies on 2-phenylethyl- N,N -dimethylamine and it is based on the hypothesis that to form an immonium dication the probe pulse is absorbed by electrons on the NH_2 . The TD-DFT calculation of Ref. 10 partially confirms this hypothesis, finding that the NH_2 hole density oscillates mainly at frequency $\Omega_2^{\text{DFT}} \approx 0.36$ PHz for $\tau \lesssim 14$ fs and $\Omega_1^{\text{DFT}} \approx 0.25$ PHz for $\tau \gtrsim 14$ fs. However, in addition to the mismatch between Ω_2^{exp} and Ω_2^{DFT} , no clear evidence of the slow dominant oscillation at frequency Ω_0^{exp} was found.

The main finding of this work is that the inclusion of

dynamical correlations through the proposed NEGF approach is crucial to achieve a quantitative overall agreement with the experimental data. In particular, dynamical correlations are responsible for the appearance of a dominant oscillation at frequency $\Omega_0 \approx 0.15$ PHz, for the renormalization of the high frequency Ω_2 (≈ 0.34 PHz in mean-field and ≈ 0.30 PHz in NEGF), and for the transition at delay $\tau \approx 14$ fs from bichromatic to monochromatic behavior with frequency $\Omega_1 \approx 0.25$ PHz.

We examine the most abundant conformer of the aminoacid phenylalanine¹⁰ which consists of a central CH unit linked to an amine group ($-\text{NH}_2$), a carboxylic group ($-\text{COOH}$) and a benzyl group ($-\text{CH}_2\text{C}(\text{CH}_3)_5$). We consider a linearly polarized XUV pulse with a weak peak intensity $I_{\text{pump}} = 5 \times 10^{11} \text{ W/cm}^2$ (ensuring a linear response behavior), central photon energy $\omega_{\text{pump}} = 30 \text{ eV}$ and duration $\tau_{\text{pump}} = 300 \text{ as}$ (with a \sin^2 envelope) yielding photon energies in the range $\sim (15, 45) \text{ eV}$. Since the phenylalanine molecules of the experimentally generated plume are randomly oriented we perform calculations for light polarization along the x, y, z directions and average the results. The XUV-induced ionization and the subsequent ultrafast charge migration are numerically simulated using the CHEERS@Yambo code^{47,48} that solves the NEGF equation for the single-particle density matrix $\rho(t)$ in KS basis at fixed nuclei. Multiple ionization channels are taken into account by an exact *embedding* procedure for the KS continuum states while dynamical correlations enter through a collision integral, which is a functional of ρ at all previous times. Details on the theoretical method and numerical implementation are provided in the Supporting Information.

To highlight the role of dynamical correlations we solve the NEGF equation in the (mean-field) Hartree-Fock (HF) approximation and in the (beyond mean-field) second Born (2B) approximation. The latter has been shown to be accurate for equilibrium spectral properties⁴⁹ and total energies⁵⁰ of several molecules. More importantly for the present work, the 2B approximation faithfully reproduces the nonequilibrium behavior of finite and not too strongly correlated systems (like the phenylalanine molecule considered here). This evidence emerges from benchmarks against numerically exact simulations in 1D atoms and molecules,⁵¹ quantum wells,⁵² weakly correlated Hubbard and extended Hubbard nanoclusters,^{53–58} the Anderson model at finite bias⁵⁹ and photo-excited donor-acceptor tight-binding Hamiltonians.⁶⁰ The fixed nuclei approximation is not expected to be too severe either (this is confirmed *a posteriori* by Fig. 2). Considering the molecular structure in Fig. 1, the time-dependent variation of the electronic charge on the amine group is due to electron flow through the N-C bond. The N-C stretching mode is medium-weak and it has a period of about $25 \div 30 \text{ fs}$; hence the electron dynamics up to 30 fs is not too disturbed by this mode. Furthermore, nonadiabatic couplings become less important when the cationic wavepacket is a linear combination of several many-electron states spread over a

broad energy range. This is precisely the situation of the experiment in Ref. 10 since the bandwidth of the ionizing XUV is as large as 30 eV.

After ionization, the coherent superposition of cationic states is characterized by several fs and sub-fs oscillations. Following the suggestion of Refs. 10,46 we have calculated the TD charge $N_{\text{amine}}(t)$ on the amine group by integrating the electron density in the light-yellow box shown in Fig. 1. The box was carefully chosen to give the correct number of valence electrons in equilibrium, i.e., $N_{\text{amine}}(0) = 7$. In analogy with the analysis of Ref. 10 we perform a sliding-window Fourier transform of the relative variation of $N_{\text{amine}}(t)$ with respect to its time-averaged value $\langle N_{\text{amine}} \rangle$

$$\tilde{N}_{\text{amine}}(\tau_d, \omega) = \int dt e^{-i\omega t} e^{-(t-\tau_d)^2/t_0^2} \delta N_{\text{amine}}(t), \quad (1)$$

where $\delta N_{\text{amine}}(t) \equiv N_{\text{amine}}(t) - \langle N_{\text{amine}} \rangle$ and $t_0 = 10$ fs. The resulting spectrograms are shown in Fig. 2 panel (b) (2B) and panel (c) (HF). The theoretical spectra are compared with the spectrogram of the experimental yield in panel (a). The latter has been obtained as in Eq. (1) after replacing $\delta N_{\text{amine}}(t)$ with the yield $Y(t)$ taken from Ref. 10.

The agreement between the 2B spectrogram and the experimental one is astounding. For $\tau_d \lesssim 15$ fs they both exhibit two main structures almost at the same frequencies: $\Omega_0 \approx 0.15$ PHz and $\Omega_2 \approx 0.30$ PHz (theory), $\Omega_0^{\text{exp}} \approx 0.14$ PHz and $\Omega_2^{\text{exp}} \approx 0.30$ PHz (experiment). Remarkably, the 2B calculation reproduces the relative weight as well, the peak at lower frequency being much more pronounced. At $\tau_d \approx 15$ fs a bichromatic-monochromatic transition occurs, and again the 2B frequency $\Omega_1 \approx 0.25$ PHz is very close to the experimental one $\Omega_1^{\text{exp}} \approx 0.24$ PHz. Of course, as we are comparing the TD amine density with the TD yield of immonium dications, a quantitative agreement in terms of peak intensities, delays, etc. cannot be, in principle, expected. Nonetheless, our results strongly corroborates the hypothesis of Ref. 10 according to which the two quantities are tightly related. In Fig. 3 we display snapshots of the real-space distribution of the molecular charge at three times corresponding to a maximum, consecutive minimum and then maximum of $N_{\text{amine}}(t)$ before (top) and after (bottom) the transition at $\tau_d \approx 15$ fs. The dominant oscillations at frequency $\Omega_0 \approx 0.15$ PHz (period 6.7 fs) and $\Omega_1 \approx 0.25$ PHz (period 4.0 fs) are clearly visible. Interestingly, the periodic motion of the charge on the amine group is not followed by other regions of the molecule. This is a further indication of the role played by the quantity $N_{\text{amine}}(t)$ in predicting the probe-induced molecular fragmentation.

The impact of dynamical correlations can be clearly appreciated in Fig. 2 (c) where the spectrogram resulting from the mean-field HF approximation is shown. Overall, the agreement with the experimental spectrogram is rather poor. We have a single dominant frequency $\Omega_1^{\text{HF}} \approx 0.26$ PHz appearing at $\tau_d \approx 12$ fs. Subdom-

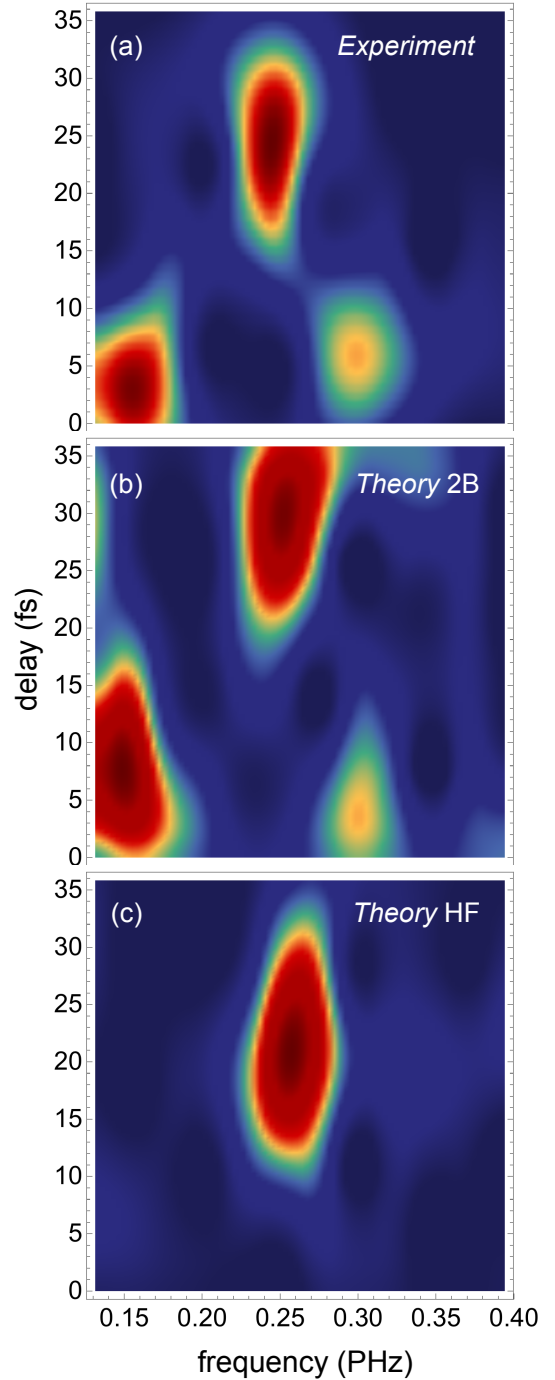


FIG. 2. Spectrograms of (a) experimental yield $Y(\tau)$ of immonium dications (row data from Fig. S4 of Ref. 10) (b-c) variation $\delta N_{\text{amine}}(t)$ of the charge on the amine group calculated within the 2B approximation (b) and HF approximation (c). All spectrograms are obtained by performing a Fourier transform with a sliding gaussian window-function of width 10 fs centered at delay τ_d (vertical axis), see Eq. (1).

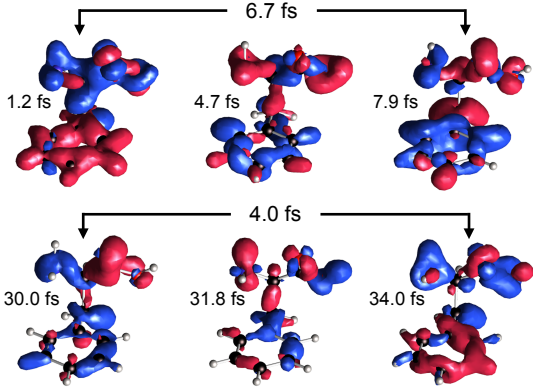


FIG. 3. Snapshots of the real-space distribution of the molecular charge at three times corresponding to a maximum, consecutive minimum and then maximum of $\delta N_{\text{amine}}(t)$ before (top) and after (bottom) the transition at $\tau_d \approx 15$ fs. The snapshots highlight the two most prominent oscillations at $\Omega_0 \approx 0.15$ PHz (period 6.7 fs) and $\Omega_2 \approx 0.25$ PHz (period 4.0 fs) observed in the correlated spectrogram of Fig. 2 (b). Hole excess (blue) and electron excess (red) are with respect to the reference density obtained by averaging $\rho(t)$ over the full real-time simulation.

inant structures of frequencies $\Omega_0^{\text{HF}} \approx 0.12$ PHz and $\Omega_2^{\text{HF}} \approx 0.34$ PHz exist too but are not visible.

In fact, the height of the corresponding peaks is at least 2.5 times smaller than that of the dominant one [see also Fig. 5 (c)]. In the Supporting Information we display the 3D plot of all three spectrograms to better appreciate the relative weight of the various structures.

To get further insight into the dynamics of ultrafast charge migration, let us denote by $\text{HF}m$, $m = 1, \dots, 32$, the HF orbitals of the 64 valence electrons of the phenylalanine (ordered according to increasing values of the HF energy, hence HF32 is the HOMO). In NEGF calculations the HF basis is special since the HF orbitals are fully occupied or empty in the HF approximation and hence these are the reference orbitals to identify correlation effects like double or multiple excitations⁴¹. In Fig. 4 (a) we have singled out those $\text{HF}m$ with a sizable amplitude on the amine group. We show the square modulus of their wavefunctions along with the value (upper-left corner) of the respective spatial integrals over the light-yellow box of Fig. 1. Figure 4 (b) contains the Fourier transform of the single-particle density matrix $\rho_{ij}(t)$ for the most relevant excitations $\text{HF}i \leftrightarrow \text{HF}j$. We display separately two spectral regions, one close to $\Omega_0 = 0.15$ PHz (left) and the other close to $\Omega_2 \approx 0.30$ PHz (right). The results have been obtained using the 2B and HF approximations and by averaging over the three orthogonal polarizations of the XUV pulse (more details are provided in Supporting Information). The low frequency Ω_0 is due to three (almost) degenerate excitations, namely $\text{HF}13 \leftrightarrow \text{HF}14$, $\text{HF}18 \leftrightarrow \text{HF}19$ and $\text{HF}19 \leftrightarrow \text{HF}20$, and the left panel of Fig. 4 (b) shows the sum of them. In HF these excitations are slightly red-shifted, $\Omega_0^{\text{HF}} = 0.12$ PHz, and

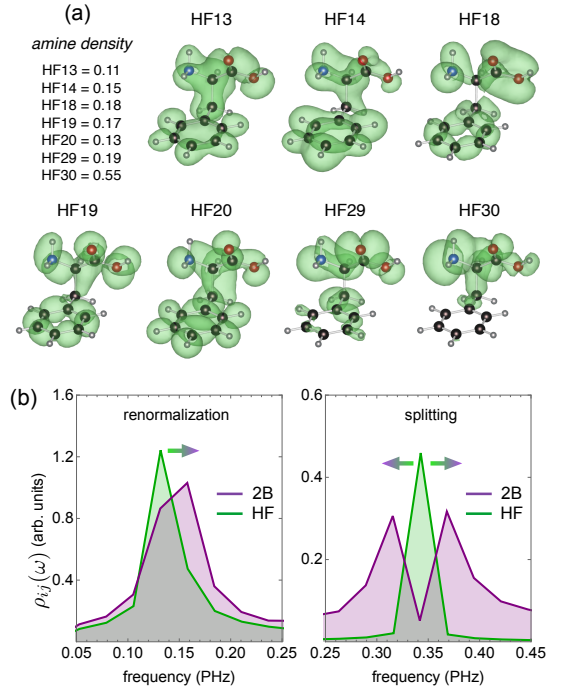


FIG. 4. Panel (a): Real-space plot of the HF orbitals with sizable charge on the amine group (see upper-left corner). Panel (b): Fourier transform of selected elements of the single-particle density matrix $\rho_{ij}(t)$ in the HF basis for frequencies close to Ω_0 (left) and Ω_2 (right). The low frequency Ω_0 is due to three (almost) degenerate excitations, namely $\text{HF}13 \leftrightarrow \text{HF}14$, $\text{HF}18 \leftrightarrow \text{HF}19$ and $\text{HF}19 \leftrightarrow \text{HF}20$ and the left plot shows $\sum_{(i,j)} |\rho_{ij}(\omega)|$ with $(i,j) = (13,14), (18,19), (19,20)$. The high frequency Ω_2 is due to the excitation $\text{HF}29 \leftrightarrow \text{HF}30$ and the right plot shows $|\rho_{29,30}(\omega)|$. To obtain $\rho(t)$ we have performed calculations in the HF and 2B approximations for the three orthogonal polarizations of the XUV pulse and then we have averaged the results.

the corresponding peak is hardly visible in the spectrogram of Fig. 2 (c). Dynamical (2B) correlations redistributes substantially the spectral weight and give rise to a renormalization of about 0.03 PHz (0.12 eV), moving the low frequency much closer to the experimental value. The high frequency Ω_2 is due to the excitation $\text{HF}29 \leftrightarrow \text{HF}30$. The involved HF orbitals are those with the largest amplitude on the amine group, in agreement with Ref. 10. In the HF calculation the $\text{HF}29 \leftrightarrow \text{HF}30$ excitation occurs at $\Omega_2^{\text{HF}} \approx 0.34$ PHz (TD-DFT predicts a slightly larger value ≈ 0.36 PHz¹⁰) and, as the low frequency excitation, it is not detected by the spectrogram, see Fig. 2 (c). The effect of dynamical (2B) correlations is to split Ω_2^{HF} into a doublet with $\Omega_2^+ \approx 0.38$ PHz and $\Omega_2^- \approx 0.30$ PHz, suggesting that the underlying excitations are actually double excitations^{41,53}. Moreover, the redistribution of spectral weight makes visible only the structure at Ω_2 , in excellent agreement with the experimental spectrogram. We mention that the central dominant frequency $\Omega_1 = 0.25$ PHz, see Fig. 2, depends only

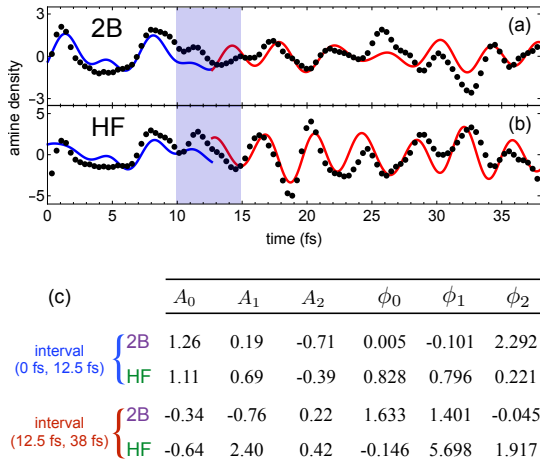


FIG. 5. Panel (a) and (b): Relative variation $\delta N_{\text{amine}}(t)$ ($\times 10^6$) after filtering out all oscillations faster than 0.4 PHz, obtained within the 2B and HF approximations (dotted curves). Solid curves are trichromatic best fits obtained with the function $\sum_{i=0}^2 A_i \sin(\Omega_i t + \phi_i)$ in the time window (0 fs, 12.5 fs) (blue) and (12.5 fs, 38 fs) (red). Panel (c): Best fitted amplitudes A_i (scaled by a factor 10^6) and phases ϕ_i

weakly on electronic correlations since it occurs at almost the same energy and delay τ_d in the 2B, HF and TD-DFT¹⁰. In our simulations this frequency should be assigned to the HF18 \leftrightarrow HF20 excitation. See Supporting Information for more details.

We finally address the transition around 10 \div 15 fs leading to the suppression of the structures at Ω_0 and Ω_2 and the concomitant development of the central structure at Ω_1 . We consider the 2B and HF curve $\delta N_{\text{amine}}(t)$ shown in Fig. 5 (dotted) and perform two different trichromatic fits with the function $\sum_{i=0}^2 A_i \sin(\Omega_i t + \phi_i)$ in the time intervals (0 fs, 12.5 fs) and (12.5 fs, 38 fs), see blue and red curves respectively. The fitting parameters are the amplitudes and phases whereas the frequencies are Ω_i in 2B, panel (a), and Ω_i^{HF} in HF, panel (b). The values of A_i and ϕ_i are reported in panel (c). We clearly see a dramatic change of the fitted amplitudes across the transition around 10 \div 15 fs, consistent with the spectrograms of Fig. 2.

In conclusion, we proposed a first-principles NEGF approach to study ultrafast charge migration during and after the action of an ionizing XUV pulse on the phenylalanine molecule. Multiple ionization channels of the initially correlated many-electron system were taken into account through an exact *embedding* procedure for the

KS states in the continuum. Dynamical correlation effects were included at the level of the self-consistent second Born approximation, thus incorporating double excitations and other scattering mechanisms in the electron dynamics. The obtained results indicate that dynamical correlations (and hence memory effects) are crucial to achieve a quantitative agreement with the experimental data. In fact, although the charge density oscillation of frequency Ω_1 at delays larger than $\tau_d \approx 15$ fs is captured even in HF, the mean-field results do not display any significant structure at smaller delays. On the contrary, the correlated NEGF calculations show a substantial reshaping, characterized by the monochromatic-bichromatic transition $\Omega_1 \leftrightarrow (\Omega_0, \Omega_2)$. All frequencies as well as the delay of the transition are in excellent agreement with the experiment. The overall similarity between the theoretical and experimental spectrograms corroborates the existence of a tight relation between the charge on the amine group and the yield of immonium dications.

We finally observe that the NEGF approach proposed here can be extended in at least two different ways to include the effects of nuclear motion. The first is through the Ehrenfest approximation and it requires to update the one-particle and two-particle integrals during the time-propagation. The second stems from many-body perturbation theory and it consists in adding the Fan self-energy⁶¹ with equilibrium vibronic propagators to the electronic correlation self-energy. These developments allow for incorporating either classical effects or quantum harmonic effects, thus opening the door to studies of a broader class of phenomena.

ACKNOWLEDGMENTS

We thank P. Decleva for providing us with the nuclear coordinates of the most abundant conformer of the phenylalanine molecule. G.S. and E.P. acknowledge EC funding through the RISE Co-ExAN (Grant No. GA644076). A.M., D.S., and E.P. also acknowledge funding from the European Union project MaX Materials design at the eXascale H2020-EINFRA-2015-1, Grant Agreement No. 676598 and Nanoscience Foundries and Fine Analysis-Europe H2020-INFRAIA-2014-2015, Grant Agreement No. 654360. G.S. and E.P. acknowledge the computing facilities provided by the CINECA Consortium within IscrCAIRETID and the INFN17_nemesys project under the CINECA-INFN agreement.

* gianluca.stefanucci@roma2.infn.it

¹ F. Krausz and M. Ivanov, Rev. Mod. Phys. **81**, 163 (2009).

² F. Gao and O. Inganäs, Phys. Chem. Chem. Phys. **16**, 20291 (2014).

³ P. Song, Y. Li, F. Ma, T. Pullerits, and M. Sun, Chem. Rec. **16**, 734 (2016).

⁴ C. A. Rozzi, F. Troiani, and I. Tavernelli, J. Phys.: Condens. Matter **30**, 013002 (2018).

- ⁵ M. Nisoli, P. Decleva, F. Calegari, A. Palacios, and F. Martín, *Chem. Rev.* **117**, 10760 (2017).
- ⁶ V. May and O. Kühn, *Charge and energy transfer dynamics in molecular systems* (John Wiley & Sons, 2008).
- ⁷ C. Andrea Rozzi, S. Maria Falke, N. Spallanzani, A. Rubio, E. Molinari, D. Brida, M. Maiuri, G. Cerullo, H. Schramm, J. Christoffers, and *et al.*, *Nat. Commun.* **4**, 1602 (2013).
- ⁸ S. M. Falke, C. A. Rozzi, D. Brida, M. Maiuri, M. Amato, E. Sommer, A. De Sio, A. Rubio, G. Cerullo, E. Molinari, and *et al.*, *Science* **344**, 1001 (2014), <http://science.sciencemag.org/content/344/6187/1001.full.pdf>.
- ⁹ A. I. Kuleff and L. S. Cederbaum, *J. Phys. B: At. Mol. Phys.* **47**, 124002 (2014).
- ¹⁰ F. Calegari, D. Ayuso, A. Trabattoni, L. Belshaw, S. De Camillis, S. Anumula, F. Frassetto, L. Poletto, A. Palacios, P. Decleva, and *et al.*, *Science* **346**, 336 (2014), <http://science.sciencemag.org/content/346/6207/336.full.pdf>.
- ¹¹ P. M. Kraus, B. Mignolet, D. Baykusheva, A. Rupenyan, L. Horný, E. F. Penka, G. Grassi, O. I. Tolstikhin, J. Schneider, F. Jensen, and *et al.*, *Science* (2015), 10.1126/science.aab2160, <http://science.sciencemag.org/content/early/2015/10/21/science.1240020.full.pdf>.
- ¹² K.-J. Yuan, C.-C. Shu, D. Dong, and A. D. Bandrauk, *J. Phys. Chem. Lett.* **8**, 2229 (2017), <http://dx.doi.org/10.1021/acs.jpclett.7b00877>.
- ¹³ M. Drescher, M. Hentschel, R. Kienberger, M. Uiberacker, V. Yakovlev, A. Scrinzi, T. Westerwalbesloh, U. Kleineberg, U. Heinzmann, and F. Krausz, *Nature* **419**, 803 (2002).
- ¹⁴ M. Schultze, M. Fieß, N. Karpowicz, J. Gagnon, M. Korbman, M. Hofstetter, S. Neppl, A. L. Cavalieri, Y. Komninos, T. Mercouris, and *et al.*, *Science* **328**, 1658 (2010), <http://science.sciencemag.org/content/328/5986/1658.full.pdf>.
- ¹⁵ M. Uiberacker, T. Uphues, M. Schultze, A. J. Verhoef, V. Yakovlev, M. F. Kling, J. Rauschenberger, N. M. Kabachnik, H. Schröder, M. Lezius, and *et al.*, *Nature* **446**, 627 (2007).
- ¹⁶ L. Belshaw, F. Calegari, M. J. Duffy, A. Trabattoni, L. Poletto, M. Nisoli, and J. B. Greenwood, *J. Phys. Chem. Lett.* **3**, 3751 (2012), <http://dx.doi.org/10.1021/jz3016028>.
- ¹⁷ E. Runge and E. K. U. Gross, *Phys. Rev. Lett.* **52**, 997 (1984).
- ¹⁸ C. Ullrich, *Time-Dependent Density-Functional Theory* (Oxford University Press, Oxford, 2012).
- ¹⁹ P. Wopperer, U. De Giovannini, and A. Rubio, *Eur. Phys. J. B* **90**, 51 (2017).
- ²⁰ U. De Giovannini, G. Brunetto, A. Castro, J. Walkenhorst, and A. Rubio, *ChemPhysChem* **14**, 1363 (2013).
- ²¹ T. Kuś, B. Mignolet, R. D. Levine, and F. Remacle, *J. Phys. Chem. A* **117**, 10513 (2013), <http://dx.doi.org/10.1021/jp407295t>.
- ²² D. Ayuso, A. Palacios, P. Decleva, and F. Martín, *Phys. Chem. Chem. Phys.* **19**, 19767 (2017).
- ²³ M. Lara-Astiaso, D. Ayuso, I. Tavernelli, P. Decleva, A. Palacios, and F. Martín, *Faraday Discuss.* **194**, 41 (2016).
- ²⁴ A. Bruner, S. Hernandez, F. Mauger, P. M. Abanador, D. J. LaMaster, M. B. Gaarde, K. J. Schafer, and K. Lopata, *J. Phys. Chem. Lett.* **8**, 3991 (2017), <http://dx.doi.org/10.1021/acs.jpclett.7b01652>.
- ²⁵ D. Cho, J. R. Rouxel, M. Kowalewski, J. Y. Lee, and S. Mukamel, *J. Chem. Theory Comput.* **14**, 329 (2018), <https://doi.org/10.1021/acs.jctc.7b00920>.
- ²⁶ L. Cederbaum and J. Zobeley, *Chem. Phys. Lett.* **307**, 205 (1999).
- ²⁷ F. Remacle and R. D. Levine, *Proc. Natl. Acad. Sci. U. S. A.* **103**, 6793 (2006), <http://www.pnas.org/content/103/18/6793.full.pdf>.
- ²⁸ H. Hennig, J. Breidbach, and L. S. Cederbaum, *J. Phys. Chem. A* **109**, 409 (2005), <http://dx.doi.org/10.1021/jp046232s>.
- ²⁹ N. T. Maitra, F. Zhang, R. J. Cave, and K. Burke, *J. Chem. Phys.* **120**, 5932 (2004).
- ³⁰ S. Kümmel and L. Kronik, *Rev. Mod. Phys.* **80**, 3 (2008).
- ³¹ E. Perfetto, A.-M. Uimonen, R. van Leeuwen, and G. Stefanucci, *Phys. Rev. A* **92**, 033419 (2015).
- ³² O. Gritsenko and E. J. Baerends, *J. Chem. Phys.* **121**, 655 (2004).
- ³³ N. T. Maitra and D. G. Tempel, *J. Chem. Phys.* **125**, 184111 (2006).
- ³⁴ J. I. Fuks and N. T. Maitra, *Phys. Rev. A* **89**, 062502 (2014).
- ³⁵ J. B. Neaton, M. S. Hybertsen, and S. G. Louie, *Phys. Rev. Lett.* **97**, 216405 (2006).
- ³⁶ K. S. Thygesen and A. Rubio, *Phys. Rev. Lett.* **102**, 046802 (2009).
- ³⁷ P. Myöhänen, R. Tuovinen, T. Korhonen, G. Stefanucci, and R. van Leeuwen, *Phys. Rev. B* **85**, 075105 (2012).
- ³⁸ C. S. Cucinotta, D. Hughes, and P. Ballone, *Phys. Rev. B* **86**, 045114 (2012).
- ³⁹ L. P. Kadanoff and G. A. Baym, *Quantum statistical mechanics: Green's function methods in equilibrium and nonequilibrium problems* (Benjamin, 1962).
- ⁴⁰ P. Danielewicz, *Ann. Phys.* **152**, 239 (1984).
- ⁴¹ G. Stefanucci and R. van Leeuwen, *Nonequilibrium Many-Body Theory of Quantum Systems: A Modern Introduction* (Cambridge University Press, Cambridge, 2013).
- ⁴² A. Stan, N. E. Dahlen, and R. van Leeuwen, *J. Chem. Phys.* **130**, 224101 (2009), <https://doi.org/10.1063/1.3127247>.
- ⁴³ K. Balzer and M. Bonitz, *Nonequilibrium Green's Functions Approach to Inhomogeneous Systems* (Springer, 2012).
- ⁴⁴ P. Lipavský, V. Špička, and B. Velický, *Phys. Rev. B* **34**, 6933 (1986).
- ⁴⁵ S. Latini, E. Perfetto, A.-M. Uimonen, R. van Leeuwen, and G. Stefanucci, *Phys. Rev. B* **89**, 075306 (2014).
- ⁴⁶ L. Lehr, T. Horneff, R. Weinkauff, and E. Schlag, *J. Phys. Chem. A* **109**, 8074 (2005).
- ⁴⁷ CHEERS@Yambo is an ongoing project stored in a dedicated private repository under the Yambo organization on GitHub, See Ref. 62.
- ⁴⁸ E. Perfetto and G. Stefanucci, in preparation.
- ⁴⁹ M. Schüler and Y. Pavlyukh, arXiv:1710.08660 (2017).
- ⁵⁰ N. E. Dahlen and R. van Leeuwen, *J. Chem. Phys.* **122**, 164102 (2005), <https://doi.org/10.1063/1.1884965>.
- ⁵¹ K. Balzer, S. Bauch, and M. Bonitz, *Phys. Rev. A* **82**, 033427 (2010).
- ⁵² K. Balzer, S. Hermanns, and M. Bonitz, *EPL (Europhysics Letters)* **98**, 67002 (2012).
- ⁵³ N. Säkkinen, M. Manninen, and R. van Leeuwen, *New J. Phys.* **14**, 013032 (2012).
- ⁵⁴ S. Hermanns, N. Schlünzen, and M. Bonitz, *Phys. Rev. B* **90**, 125111 (2014).
- ⁵⁵ N. Schlünzen and M. Bonitz, *Contrib. Plasma Phys.* **56**, 5 (2016).

- ⁵⁶ M. Hopjan, D. Karlsson, S. Ydman, C. Verdozzi, and C.-O. Almbladh, Phys. Rev. Lett. **116**, 236402 (2016).
- ⁵⁷ Y. B. Lev and D. R. Reichman, EPL (Europhysics Letters) **113**, 46001 (2016).
- ⁵⁸ N. Schlünzen, J.-P. Joost, F. Heidrich-Meisner, and M. Bonitz, Phys. Rev. B **95**, 165139 (2017).
- ⁵⁹ A.-M. Uimonen, E. Khosravi, A. Stan, G. Stefanucci, S. Kurth, R. van Leeuwen, and E. K. U. Gross, Phys. Rev. B **84**, 115103 (2011).
- ⁶⁰ E. V. Boström, A. Mikkelsen, C. Verdozzi, E. Perfetto, and G. Stefanucci, Nano Lett. **18**, 785 (2018), <https://doi.org/10.1021/acs.nanolett.7b03995>.
- ⁶¹ H. Y. Fan, Phys. Rev. **82**, 900 (1951).
- ⁶² A. Marini, C. Hogan, M. Grüning, and D. Varsano, Comput. Phys. Commun. **180**, 1392 (2009).